VIP Electrochemistry Very Important Paper

International Edition: DOI: 10.1002/anie.201508199
German Edition: DOI: 10.1002/ange.201508199

Energy-Level Alignment for Single-Molecule Conductance of Extended Metal-Atom Chains

Ta-Cheng Ting, Liang-Yan Hsu, Min-Jie Huang, Er-Chien Horng, Hao-Cheng Lu, Chan-Hsiang Hsu, Ching-Hong Jiang, Bih-Yaw Jin, Shie-Ming Peng,* and Chun-hsien Chen**

Abstract: *The use of single-molecule junctions for various functions constitutes a central goal of molecular electronics. The functional features and the efficiency of electron transport are dictated by the degree of energy-level alignment (ELA), that is, the offset potential between the electrode Fermi level and the frontier molecular orbitals. Examples manifesting ELA are rare owing to experimental challenges and the large energy barriers of typical model compounds. In this work, single-molecule junctions of organometallic compounds with five metal centers joined in a collinear fashion were analyzed. The single-molecule i–V scans could be conducted in a reliable manner, and the E_{FMO} levels were electrochemically accessible. When the electrode Fermi level (E_F) is close to the frontier orbitals (E_{FMO}) of the bridging molecule, larger conductance was observed. The smaller $|E_F-E_{FMO}|$ gap was also derived quantitatively, unambiguously confirming the ELA. The mechanism is described in terms of a two-level model involving co-tunneling and sequential tunneling processes.*

Electron transport is an essential theme across major disciplines and is of utmost importance to the success of molecule-based electronic devices. For further improving such systems, an understanding of the interfacial transport processes, which can be analyzed in terms of the energy-level alignment (ELA), is crucial.[1] A small barrier height (ϕ_B), that is, the difference between the electrode Fermi level (E_F) and the frontier molecular orbitals (E_{FMO}), is expected to lead to facile transport. The degree of ELA for thin-film devices is typically unveiled by ultraviolet photoelectron spectroscopy (UPS).[1] However, for ultimate miniaturization down to the single-molecule level, the relatively large beam size of UPS renders it unsuitable for probing local structures. Moreover, each single-molecule junction confers only one ϕ_B. The lack of systematic changes in ϕ_B makes the correlation with electron-transport efficiency difficult. To this end, E_{FMO} can be shifted with a gate electrode by the field effect with single-molecule transistors (SMTs).[2] Unfortunately, SMT studies are very limited owing to fabrication difficulties. Scanning tunneling microscopy (STM) based break junctions have been shown to be a convenient method for creating single-molecule junctions,[3] and the tuning of E_F and ϕ_B is achievable through electrochemical control (hereafter referred to as EC-STM BJ) by driving the potential of the working electrode (E_{wk}) against that of the reference electrode.[4–8] Thus far, the effect of ϕ_B on the single-molecule conductance has only been proposed sporadically.[6–9] Most EC-STM BJ studies were performed at fixed E_{wk} values and unable to monitor the system upon E_F approaching E_{FMO}.

EC studies of single-molecule conductance focus mostly on organic redox moieties.[5,7–10] Examples of organometallic compounds are rare and limited to those with one[11–13] or two[14,15] metal centers, such as ferrocenedicarboxylate,[13] ferrocenedithiol,[11,12] and osmium[11] or ruthenium[14] complexes ligated by bis(terpyridine). Extended metal-atom chains (EMACs, Figure 1a)[16–18] represent a unique category of stable, electroactive, and one-dimensional wires with metal atoms robustly interwoven by metal–metal and metal–ligand bonds.[16–20] With this framework, a wide range of physicochemical properties can be achieved. For example, the strength of the metal–metal interactions depends on the number of d electrons[21] and can be tuned by selecting/mixing various transition-metal atoms,[7,20] by the use of specific ligands to reduce/oxidize the coordinated metal centers, or by chemical reactions with oxidants.[17,18] Electrochemistry is an alternative method to adjust the degree of d orbital electronic coupling between neighboring metal atoms, the E_{FMO} values, and consequently the molecular conductance. EMACs exhibit well defined redox waves within accessible potential windows.[16,17] Thus, EMACs constitute an ideal platform to manifest ELA characteristics by EC gating. Herein, the single-molecule conductance of Ni, Co, and Cr EMACs, which were used as prototypical compounds, is studied by in situ EC-STM BJ (Figure 1b). The signature of ELA was unambiguously characterized by EC-gated *i–V* curves, and the conductance behavior will be analyzed by simulations involving co-tunneling and sequential tunneling mechanisms.

The single-molecule conductance of pentametallic EMACs was determined by EC-STM BJ at fixed E_{wk} (Table 1; for experimental details, see the Supporting Information). The EC results are consistent with our previous study[19] where the oxidized EMACs were prepared by chemical oxidation of the neutral forms. Hence, the afore-

[*] T.-C. Ting, Dr. L.-Y. Hsu, Dr. M.-J. Huang, E.-C. Horng, Dr. H.-C. Lu, C.-H. Hsu, Dr. C.-H. Jiang, Prof. B.-Y. Jin, Prof. S.-M. Peng, Prof. C.-h. Chen
Department of Chemistry and Center for Emerging Material and Advanced Device
National Taiwan University
1, Sec. 4, Roosevelt Road, Taipei, 10617 (Taiwan)
E-mail: byjin@ntu.edu.tw
smpeng@ntu.edu.tw
chhchen@ntu.edu.tw
Prof. S.-M. Peng
Institute of Chemistry, Academia Sinica
Taipei, 11529 (Taiwan)

Supporting information and ORCID(s) from the author(s) for this article are available on the WWW under http://dx.doi.org/10.1002/anie.201508199.

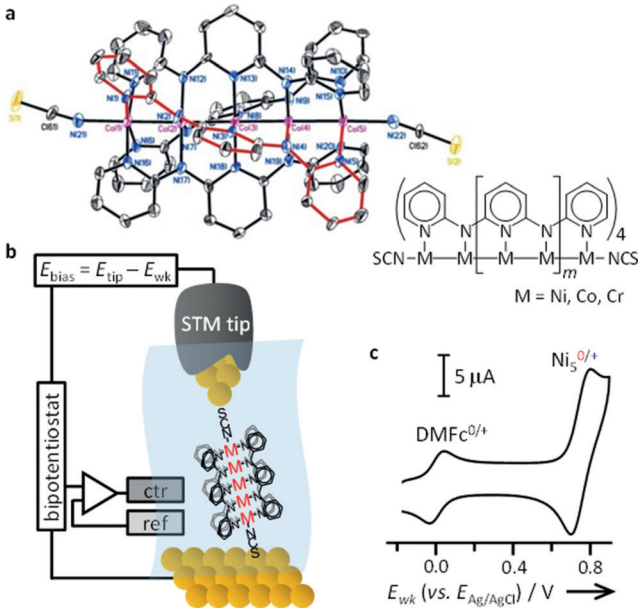

Figure 1. a) ORTEP view and schematic representation of the EMACs. The metal-atom chains were supported by four oligo-α-pyridylamido anions, $tpda^{2-}$ (tripyridyldiamido dianion; $m = 1$). One of the four equatorial ligands is highlighted in red to illustrate the helical structure. b) Experimental set-up of the EC-STM BJ measurements. c) Cyclic voltammogram of $[Ni_5(tpda)_4(NCS)_2]$. DMFc (decamethyl ferrocene) was the internal reference standard with −23 mV against $E_{Ag/AgCl}$. Other conditions: 0.1 M TBAP (tetrabutylammonium perchlorate) solution in propylene carbonate; scan rate = 100 mV s^{-1}; working electrode: glassy carbon electrode (3 mm in diameter); reference electrode: Ag wire; counterelectrode: Pt wire.

mentioned rationale that correlates metal–metal interactions with EMAC conductance also applies to the present EC study. Specifically, the ascending conductance for neutral Ni_5, Co_5, and Cr_5 EMACs is consistent with the respective bond orders of 0, 0.5, and 1.5.[19] After in situ one-electron oxidation, the conductance of the Ni_5 EMAC has increased by approximately 40% (16.4 MΩ for $[Ni_5]^0$ and 11.8 MΩ for $[Ni_5]^+$), which was ascribed to the increase in bond order resulting from the removal of one electron from an antibonding orbital. The distances between neighboring Ni atoms in the latter are shorter by 0.047 Å (from 2.294–2.371 Å in the former).[22,23] Given the minute contraction of the molecular length, the 40% increase in conductance cannot be attributed to the decrease in the tip–substrate distance. It is henceforth ascribed to the different intrinsic properties of $[Ni_5]^0$ and $[Ni_5]^+$. For the Co_5 EMAC, the conductance and the Co–Co bond order remain unchanged because the electron is removed from a nonbonding orbital.

Table 1: Single-molecule conductance ($\times 10^{-4}$ G_0) of pentametallic EMACs.[a]

	$[M_5(tpda)_4(NCS)_2]^0$		$[M_5(tpda)_4(NCS)_2]^+$
Ni	7.9 (±1.0)		10.9 (±1.5)
Co	9.1 (±1.1)		9.3 (±1.1)
Cr	48.8 (±1.0)[b]	9.5 (±1.2)[b]	10.8 (±1.3)

[a] The solvent and supporting electrolyte were propylene carbonate and 0.1 M TBAP solution, respectively. The conductance histograms are shown in Figure S6. [b] Neutral Cr_5 EMACs have two sets of single-molecule conductance peaks, which were attributed to delocalized and localized Cr–Cr interactions.

The structure of the Cr_5 EMAC and the corresponding conductance behavior are fascinating, yet complicated.[16,19,24] X-ray crystallography[23–25] and Raman spectroscopy[25,26] studies have confirmed that the neutral Cr EMAC has two types of conformations, termed the delocalized and localized forms, but the chemically oxidized product adopts exclusively the localized one (see Figure S6c). For the delocalized Cr_5 EMAC, the four Cr–Cr interactions all have bond orders of 1.5, meaning that the electrons are delocalized along the string of five Cr centers. For the other conformation, the electrons are localized within two of the four Cr–Cr pairs, which are alternatingly triple-bonded and nonbonding.[16–19,24] The neutral and oxidized forms exhibit two sets and one set of conductance values, respectively, in which the value of the oxidized form appears to be almost identical to the less conductive set of the neutral form (Table 1). Accordingly, the higher conductance of the neutral form is attributed to its delocalized nature whereas the less conductive system displays alternating bond lengths.

Although the effect of EC gating on single-molecule conductance is shown in Table 1, the values were determined at fixed E_{wk} values by conductance histograms which in practice cannot monitor the conductance continuously over a range of E_{wk} values. To disclose the individual behavior of one single molecule, G–E_{wk} traces were acquired to elucidate the single-molecule conductance as a function of E_{wk} (Figure 2). Note that the E_{bias} ($= E_{tip-wk} = E_{tip} - E_{wk}$) value was fixed by sweeping E_{tip} synchronously with E_{wk} (Figure 2a). Prior to and after the one-electron oxidation of $[Ni_5]^0$, the respective nominal conductance values are about 0.79×10^{-3} G_0 and 1.1×10^{-3} G_0 (indicated in Figure 2b), which are in a good agreement with those obtained at fixed E_{wk} values (Table 1). The conductance of $[Co_5]^{2+}$ (at > 1.0 V) is approximately 0.9×10^{-3} G_0 and thus about the same as those of $[Co_5]^0$ and $[Co_5]^+$ (at $E_{wk} = 0.6$–0.8 V; Figure 2c). As the Cr_5 EMAC has two conformations, the scan of the G–E_{wk} traces starts from the oxidized form ($E_{wk} \approx 0.5$ V) such that the same initial experimental conditions can unveil the behavior of both the localized (ca. 0.95×10^{-3} G_0; Figure 2d) and the delocalized form (ca. 5.0×10^{-3} G_0; Figure 2c). The i–E_{wk} traces of the reverse scans (i.e., from $[M_5]^+$ to $[M_5]^0$) are shown in Figure 2d,e (see Figure S8 for that of the Ni_5 EMAC). The direction of the current flow is the same as that for the forward E_{wk} scan, confirming that what is monitored is not predominantly due to the diffusional redox current of the EMACs. The variation in the peak positions sometimes reaches 0.4 V, probably owing to molecular conformations with various degrees of deformation for each junction, which cause the redox reactions to deviate from the optimal transition pathways described by the potential energy surface. Note that the second electron oxidation processes, $[M_5]^+/[M_5]^{2+}$, were also monitored, which can otherwise not be studied owing to the difficulties associated with the purification and crystallization of the chemically oxidized products.

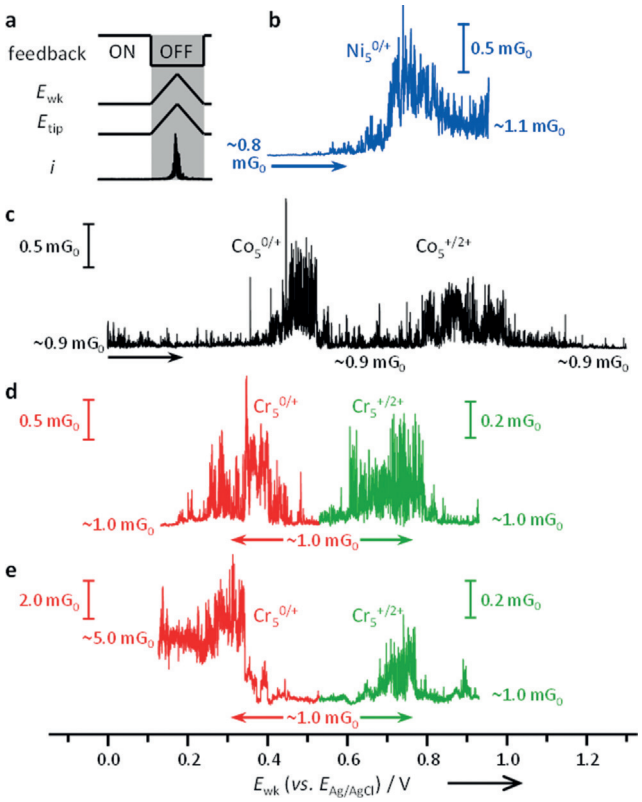

Figure 2. Determination of the energy-level alignment by continuous G–E_{wk} scans. a) Waveforms of E_{wk} and E_{tip} for the measurement of i–E_{wk} curves from single-molecule junctions of b) Ni_5, c) Co_5, d) localized Cr_5, and e) delocalized Cr_5 EMACs. After the feedback was turned off, both tip and substrate were subjected to a potential sweep, with E_{tip-wk} being fixed at 50 mV. To validate the curves, the returning current was shown to be the same as that before the potential sweep ($i_{final} \approx i_{initial}$ in (a)). The current of the i–E_{wk} traces was divided by E_{tip-wk}, which resulted in the G–E_{wk} traces. Scan rate: 5 V s^{-1} (b), 0.5 V s^{-1} (c–e). The values in mG_0 indicate the nominal conductance of the samples at either $E_{initial}$ or E_{final}. The arrows indicate the sweeping direction of E_{wk}. All other conditions were the same as those in Figure 1.

The significance of Figure 2 is that all of the traces exhibit elevated conductance and that the positions agree reasonably well with the corresponding redox potentials of the EMACs (Figure S4). The peak-shaped conductance fluctuation was therefore ascribed to the alignment of the electrode E_F with the molecular E_{FMO}. To scrutinize the mechanism of the EC gating effect on the single-molecule conductance, a two-level model involving co-tunneling and sequential-tunneling processes was utilized to describe the electron transfer at the molecular junction. Co-tunneling processes (superexchange) use a virtual intermediate state of the molecule for electron transitions whereas sequential tunneling processes (two-step electron transfer) add or remove electrons to or from the molecule during the transport of one electron from one electrode to the other. The simulations of quantum transport were carried out based on the Master equation approach combined with a two-level model (see the Supporting Information).[27] Sequential tunneling processes can be coherent or incoherent. Here, only incoherent sequential tunneling was considered because the simulation of coherent sequential tunneling remains a challenge and requires the detailed vibronic structures of the EMACs. The incoherent process occurs when full vibrational relaxation of the occupied (reduced) level is achieved, and the two-step electron transfer processes are uncorrelated.[28]

The electron-transfer processes mediated by the energy levels of the two states of the bridging molecule are illustrated in Figure 3a. When E_{wk} is very different from the redox

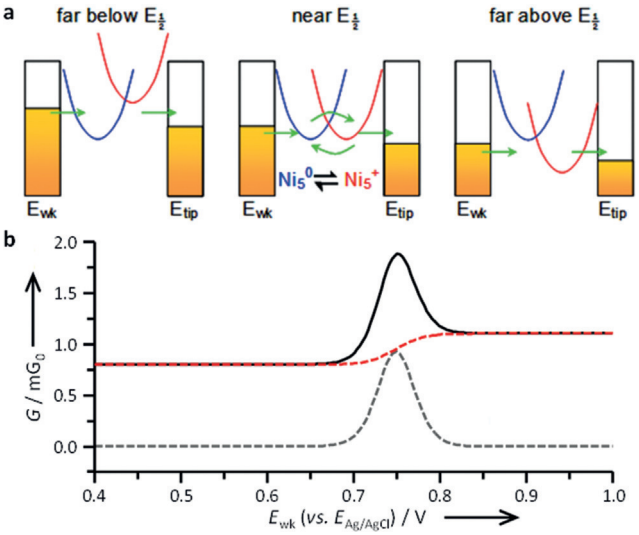

Figure 3. Proposed EC gating mechanism. a) Electron transport through an electrode/Ni_5 EMAC/electrode junction under EC control. The blue and red parabolas represent the neutral and oxidized forms, respectively. b) Calculated conductance plotted against E_{wk}. The solid black line is the sum of the conductance of co-tunneling (dashed red line) and sequential tunneling processes (dashed gray line).

potential, $E_{1/2}$, the molecule is mainly in its neutral or oxidized state. The co-tunneling process is thus predominant because the electron passes through either the neutral or the charged state of the molecule. When E_{wk} is similar to $E_{1/2}$, the redox reaction adds or removes electrons to or from the molecule. Sequential tunneling processes may come into play. The results of a modeling experiment that considers both co-tunneling and sequential tunneling processes are displayed in Figure 3b. The simulated conductance of Ni_5 is depicted by the solid curve, which resembles the experimental results (Figure 2b). The dashed traces unveil the details. The dashed red curve near $E_{1/2}$ reveals that the conductance of the co-tunneling process results from equal contributions from the neutral and oxidized forms, whereas sequential tunneling yields a peak centered at approximately 0.75 V. The conductance fluctuation shown in Figure 2 cannot be depicted in Figure 3 because the effects of molecular geometry fluctuations were not considered in the simulations. The conductance fluctuation in EC-gated transport deserves further exploration.

Transition voltage spectroscopy (TVS) provides profound information on molecular junctions by i–E_{bias} scans.[29] By plotting $\ln(i/E_{bias}^2)$ against $1/E_{bias}$ (e.g., Figure 4c), as derived from TVS, a Fowler–Nordheim (FN) plot was obtained in

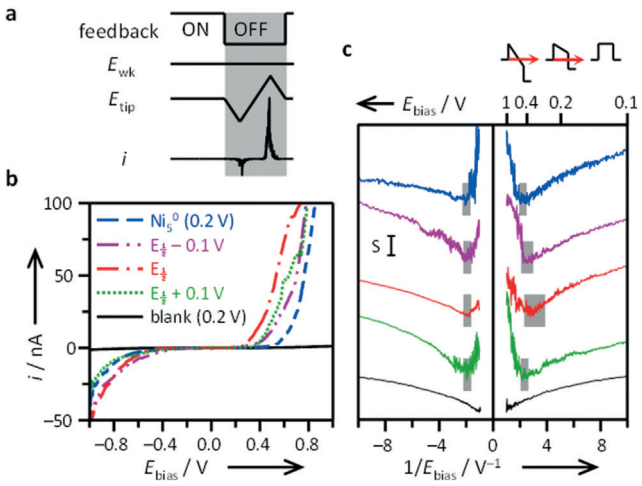

Figure 4. Transition voltage spectroscopy at EC-gated E_{wk}. a) Waveforms of the applied E_{wk} and E_{tip} for i–E_{bias} scans. b) Typical i–E_{bias} curves obtained at potentiostatted E_{wk}. Validation of the curves followed the same procedure as for the i–E_{wk} scans reported in Figure 2a ($i_{final} \approx i_{initial}$). c) Fowler–Nordheim plots of $[Ni_5(tpda)_4(NCS)_2]$ acquired at four E_{wk} values. The shaded regions indicate the distribution of V_m for each E_{wk} from more than 120 i–E_{bias} curves (Figure S7). For comparison, the black trace was acquired under EC conditions for a solution not containing Ni_5 EMACs and thus undergoing through-space tunneling. $E_{1/2}$: 0.750 V (vs. $E_{Ag/AgCl}$). Scanning rate: 5 $V s^{-1}$. Scale bar, S = 1.0 × ln(μA/V^2). All other conditions were the same as those in Figure 1.

which the minimum is termed V_m and is proximal to where the energy-level alignment takes place.[30] The FN plot can be interpreted by a potential barrier model or a molecular orbital model. Recent literature shows that the Landauer approach with a single-level molecular orbital model is more comprehensive,[30] and that the potential barrier model cannot explain the length independence of V_m.[31] Given that EMACs are very large compounds, the complicated electronic structures may lead to the overlap of multiple conduction channels, which may not be adequately described by the one-level molecular orbital model. The potential barrier model provides the effective barrier height, Φ_{effB}, which results from synergistic effects of multiple molecular orbitals and may help understand the correlation of the effective potential barrier height and EC gating. The elevated single-molecule conductance around $E_{1/2}$ (Figure 2 and Figure 3) prompted us to explore the effective tunneling barrier height, Φ_{effB}, as a function of E_{wk}. The illustration shown in Figure 4c (top),[32] although oversimplified, shows how molecular levels become accessible to the applied E_{bias} ($= E_{tip} - E_{wk}$). Therefore, V_m can be correlated to Φ_{effB}.

The i–E_{bias} curves for $[Ni_5(tpda)_4(NCS)_2]$ acquired at E_{wk} values near the redox event, including 0.65, 0.75, and 0.85 V ($E_{1/2}$ −0.10 V, $E_{1/2}$, and $E_{1/2}$ + 0.10 V) are shown in Figure 4b. The i–E_{bias} curves obtained at 0.20 V (vs. $E_{Ag/AgCl}$) represent the behavior of $[Ni_5]^0$. The E_{wk} value was held constant at the indicated potential, and the current was measured as a function of E_{bias}. These i–E_{bias} curves are asymmetric. In the high bias regime, $\ln(i/V^2)$ is proportional to $[-8\pi d(2m_e)^{1/2}\Phi_{effB}{}^{3/2}/3he](1/V)$, where d, m_e, and e are the interelectrode spacing of the molecular junction, the effective electron mass, and the elementary charge, respectively.[33] The FN plots in which $\ln(i/V^2)$ was plotted against $1/V$ are shown in Figure 4c. Note that E_{wk} was fixed, and for $E_{bias} > 0$, the scanning of E_{bias} moves E_{tip} towards or even beyond the E_{HOMO} of $[Ni_5]^0$. For $E_{bias} < 0$, the E_{tip} value approaches the E_{LUMO} of $[Ni_5]^0$.

The significance of Figure 4c is that for $E_{bias} > 0$, the value of V_m reaches a minimum of approximately 0.35 V at $E_{wk} = E_{1/2}$, consistent with optimal energy-level alignment. A larger or smaller E_{wk} results in a higher V_m. For $E_{bias} < 0$, the V_m value appears to be independent of E_{wk}, suggesting that the energy-level alignment exerts negligible effects. This finding could be explained by voltammetry measurements, which showed that the one-electron reduction of the Ni_5 EMAC takes place at −1.0 V (vs. $E_{Ag/AgCl}$; Figure S4a). With the energy difference of 1.2–2.05 V between the potentiostatted E_{wk} and that of the reduction event, the observation of similar V_m values from the i–E_{bias} curves at $E_{bias} < 0$ is plausible. The distinct dependence of V_m on the scan direction of E_{bias} further demonstrates the characteristics of the energy-level alignment by EC gating.

In conclusion, the single-molecule conductance of Ni_5, Co_5, and Cr_5 EMACs has been measured by EC-STM BJ. The additional electrochemical control obviates the need for tedious experimental procedures involving the synthesis, purification, and characterization of the chemically oxidized compounds. By taking advantage of the in situ redox reaction, the conducting behavior of the one- and two-electron-oxidized states could be explored. The continuous i–E_{wk} scans reported in this study represent a significant advancement as they enable the unambiguous analysis of the conductance behavior of Cr EMACs with delocalized Cr—Cr interactions and for those with alternating Cr—Cr bond lengths. The position of the conductance peak indicates the extent of energy-level alignment. The experimentally obtained peak-shaped i–E_{wk} curves are in good agreement with the model ones obtained by taking co-tunneling and sequential tunneling processes at $E_{wk} \approx E_{1/2}$ into account. Finally, transition voltage spectroscopy was employed for the first time to derive the V_m values of a single molecule under electrochemical control. V_m and the single-molecule conductance are strongly correlated with the proximity of E_{wk} and $E_{1/2}$, manifesting that the energy-level alignment of the electrode Fermi level with the molecular frontier orbitals is of utmost importance.

Acknowledgements

We thank Kai-Neng Shih and Professor I-Wen Peter Chen (NTTU) for the development of this project at an early stage and NTU and MOST for financial support.

Keywords: electrochemistry · electron transfer · molecular junctions · scanning tunneling microscopy

How to cite: *Angew. Chem. Int. Ed.* **2015**, *54*, 15734–15738
Angew. Chem. **2015**, *127*, 15960–15964

[1] H. Ishii, K. Sugiyama, E. Ito, K. Seki, *Adv. Mater.* **1999**, *11*, 605 – 625.
[2] H. Song, Y. Kim, Y. H. Jang, H. Jeong, M. A. Reed, T. Lee, *Nature* **2009**, *462*, 1039 – 1043.
[3] a) S. V. Aradhya, L. Venkataraman, *Nat. Nanotechnol.* **2013**, *8*, 399 – 410; b) C.-T. Kuo, L.-C. Su, C.-h. Chen, *J. Chin. Chem. Soc.* **2014**, *61*, 101 – 114; c) L. Sun, Y. A. Diaz-Fernandez, T. A. Gschneidtner, F. Westerlund, S. Lara-Avila, K. Moth-Poulsen, *Chem. Soc. Rev.* **2014**, *43*, 7378 – 7411; d) L. Chen, Y.-H. Wang, B. He, H. Nie, R. Hu, F. Huang, A. Qin, X.-S. Zhou, Z. Zhao, B. Z. Tang, *Angew. Chem. Int. Ed.* **2015**, *54*, 4231 – 4235; *Angew. Chem.* **2015**, *127*, 4305 – 4309; e) S. Afsari, Z. Li, E. Borguet, *Angew. Chem. Int. Ed.* **2014**, *53*, 9771 – 9774; *Angew. Chem.* **2014**, *126*, 9929 – 9932; f) M. Kiguchi, J. Inatomi, Y. Takahashi, R. Tanaka, T. Osuga, T. Murase, M. Fujita, T. Tada, S. Watanabe, *Angew. Chem. Int. Ed.* **2013**, *52*, 6202 – 6205; *Angew. Chem.* **2013**, *125*, 6322 – 6325.
[4] a) C. Huang, A. V. Rudnev, W. Hong, T. Wandlowski, *Chem. Soc. Rev.* **2015**, *44*, 889 – 901; b) N. Darwish, I. Díez-Pérez, P. Da Silva, N. Tao, J. J. Gooding, M. N. Paddon-Row, *Angew. Chem. Int. Ed.* **2012**, *51*, 3203 – 3206; *Angew. Chem.* **2012**, *124*, 3257 – 3260; c) Z. Li, H. Li, S. Chen, T. Froehlich, C. Yi, C. Schönenberger, M. Calame, S. Decurtins, S.-X. Liu, E. Borguet, *J. Am. Chem. Soc.* **2014**, *136*, 8867 – 8870.
[5] a) N. J. Kay, S. J. Higgins, J. O. Jeppesen, E. Leary, J. Lycoops, J. Ulstrup, R. J. Nichols, *J. Am. Chem. Soc.* **2012**, *134*, 16817 – 16826; b) J. He, Q. Fu, S. Lindsay, J. W. Ciszek, J. M. Tour, *J. Am. Chem. Soc.* **2006**, *128*, 14828 – 14835; c) X. Li, J. Hihath, F. Chen, T. Masuda, L. Zang, N. Tao, *J. Am. Chem. Soc.* **2007**, *129*, 11535 – 11542; d) E. Leary, S. J. Higgins, H. van Zalinge, W. Haiss, R. J. Nichols, S. Nygaard, J. O. Jeppesen, J. Ulstrup, *J. Am. Chem. Soc.* **2008**, *130*, 12204 – 12205.
[6] S. Guo, J. M. Artés, I. Díez-Pérez, *Electrochim. Acta* **2013**, *110*, 741 – 753.
[7] M. Baghernejad, X. Zhao, K. Baruël Ørnsø, M. Füeg, P. Moreno-García, A. V. Rudnev, V. Kaliginedi, S. Vesztergom, C. Huang, W. Hong, *J. Am. Chem. Soc.* **2014**, *136*, 17922 – 17925.
[8] a) R. J. Brooke, C. Jin, D. S. Szumski, R. J. Nichols, B.-W. Mao, K. S. Thygesen, W. Schwarzacher, *Nano Lett.* **2015**, *15*, 275 – 280; b) I. Díez-Pérez, Z. Li, S. Guo, C. Madden, H. Huang, Y. Che, X. Yang, L. Zang, N. Tao, *ACS Nano* **2012**, *6*, 7044 – 7052.
[9] B. Q. Xu, X. L. Li, X. Y. Xiao, H. Sakaguchi, N. J. Tao, *Nano Lett.* **2005**, *5*, 1491 – 1495.
[10] a) F. Chen, J. He, C. Nuckolls, T. Roberts, J. E. Klare, S. Lindsay, *Nano Lett.* **2005**, *5*, 503 – 506; b) W. Haiss, H. van Zalinge, S. J. Higgins, D. Bethell, H. Höbenreich, D. J. Schiffrin, R. J. Nichols, *J. Am. Chem. Soc.* **2003**, *125*, 15294 – 15295; c) W. Haiss, T. Albrecht, H. van Zalinge, S. J. Higgins, D. Bethell, H. Höbenreich, D. J. Schiffrin, R. J. Nichols, A. M. Kuznetsov, J. Zhang, *J. Phys. Chem. B* **2007**, *111*, 6703 – 6712; d) N. Darwish, I. Díez-Pérez, S. Guo, N. Tao, J. J. Gooding, M. N. Paddon-Row, *J. Phys. Chem. C* **2012**, *116*, 21093 – 21097.
[11] X.-S. Zhou, L. Liu, P. Fortgang, A.-S. Lefevre, A. Serra-Muns, N. Raouafi, C. Amatore, B.-W. Mao, E. Maisonhaute, B. Schöllhorn, *J. Am. Chem. Soc.* **2011**, *133*, 7509 – 7516.
[12] X. Xiao, D. Brune, J. He, S. Lindsay, C. B. Gorman, N. Tao, *Chem. Phys.* **2006**, *326*, 138 – 143.
[13] Y.-Y. Sun, Z.-L. Peng, R. Hou, J.-H. Liang, J.-F. Zheng, X.-Y. Zhou, X.-S. Zhou, S. Jin, Z.-J. Niu, B.-W. Mao, *Phys. Chem. Chem. Phys.* **2014**, *16*, 2260 – 2267.
[14] R. Davidson, J.-H. Liang, D. C. Milan, B.-W. Mao, R. J. Nichols, S. J. Higgins, D. S. Yufit, A. Beeby, P. J. Low, *Inorg. Chem.* **2015**, *54*, 5487 – 5494.
[15] A. K. Mahapatro, J. Ying, T. Ren, D. B. Janes, *Nano Lett.* **2008**, *8*, 2131 – 2136.
[16] J. F. Berry in *Multiple Bonds between Atoms* (Eds.: F. A. Cotton, C. A. Murillo, R. A. Walton), Springer Science and Business Media, Inc., New York, **2005**, p. 682.
[17] C.-Y. Yeh, C.-C. Wang, C.-h. Chen, S.-M. Peng in *Redox Systems under Nano-Space Control* (Ed.: T. Hirao), Springer-Verlag, Berlin, **2006**, pp. 85 – 116.
[18] S. A. Hua, Y. C. Tsai, S. M. Peng, *J. Chin. Chem. Soc.* **2014**, *61*, 9 – 26.
[19] I-W. P. Chen, M.-D. Fu, W.-H. Tseng, J.-Y. Yu, S.-H. Wu, C.-J. Ku, C.-h. Chen, S.-M. Peng, *Angew. Chem. Int. Ed.* **2006**, *45*, 5814 – 5818; *Angew. Chem.* **2006**, *118*, 5946 – 5950.
[20] S.-A. Hua, M.-C. Cheng, C.-h. Chen, S.-M. Peng, *Eur. J. Inorg. Chem.* **2015**, 2510 – 2523.
[21] K.-N. Shih, M.-J. Huang, H.-C. Lu, M.-D. Fu, C.-K. Kuo, G.-C. Huang, G.-H. Lee, C.-h. Chen, S.-M. Peng, *Chem. Commun.* **2010**, *46*, 1338 – 1340.
[22] a) C.-C. Wang, W.-C. Lo, C.-C. Chou, G.-H. Lee, J.-M. Chen, S.-M. Peng, *Inorg. Chem.* **1998**, *37*, 4059 – 4065; b) C.-Y. Yeh, Y.-L. Chiang, G.-H. Lee, S.-M. Peng, *Inorg. Chem.* **2002**, *41*, 4096 – 4098.
[23] S.-Y. Lin, I-W. P. Chen, C.-h. Chen, M.-H. Hsieh, C.-Y. Yeh, T.-W. Lin, Y.-H. Chen, S.-M. Peng, *J. Phys. Chem. B* **2004**, *108*, 959 – 964.
[24] J. F. Berry, F. A. Cotton, T. Lu, C. A. Murillo, B. K. Roberts, X. Wang, *J. Am. Chem. Soc.* **2004**, *126*, 7082 – 7096.
[25] C.-J. Hsiao, S.-H. Lai, I.-C. Chen, W.-Z. Wang, S.-M. Peng, *J. Phys. Chem. A* **2008**, *112*, 13528 – 13534.
[26] Y.-M. Huang, H.-R. Tsai, S.-H. Lai, S. J. Lee, I.-C. Chen, C. L. Huang, S.-M. Peng, W.-Z. Wang, *J. Phys. Chem. C* **2011**, *115*, 13919 – 13926.
[27] a) V. N. Golovach, D. Loss, *Phys. Rev. B* **2004**, *69*, 245327; b) L.-Y. Hsu, T.-W. Tsai, B.-Y. Jin, *J. Chem. Phys.* **2010**, *133*, 144705.
[28] E. P. Friis, J. E. T. Andersen, Y. I. Kharkats, R. J. Nichols, J.-D. Zhang, J. Ulstrup, *Proc. Natl. Acad. Sci. USA* **2009**, *106*, 1379 – 1384.
[29] J. M. Beebe, B. Kim, J. W. Gadzuk, C. D. Frisbie, J. G. Kushmerick, *Phys. Rev. Lett.* **2006**, *97*, 026801.
[30] a) E. H. Huisman, C. M. Guédon, B. J. van Wees, S. J. van der Molen, *Nano Lett.* **2009**, *9*, 3909 – 3913; b) M. Araidai, M. Tsukada, *Phys. Rev. B* **2010**, *81*, 235114.
[31] a) M. L. Trouwborst, C. A. Martin, R. H. M. Smit, C. M. Guédon, T. A. Baart, S. J. van der Molen, J. M. van Ruitenbeek, *Nano Lett.* **2011**, *11*, 614 – 617; b) K. Wu, M. Bai, S. Sanvito, S. Hou, *Nanotechnology* **2013**, *24*, 025203.
[32] a) J. M. Beebe, B. Kim, J. Gadzuk, C. D. Frisbie, J. G. Kushmerick, *Phys. Rev. Lett.* **2006**, *97*, 026801; b) J. M. Beebe, B. Kim, C. D. Frisbie, J. G. Kushmerick, *ACS Nano* **2008**, *2*, 827 – 832.
[33] S. Karthäuser, *J. Phys. Condens. Matter* **2011**, *23*, 013001.

Received: September 1, 2015
Published online: November 5, 2015

